İSTANBUL UNIVERSITY CERRAHPAŞA

ORIGINAL ARTICLE
Electrica 2022; 22(1): 70-83

Quasi ZSI-Fed Sliding Mode Control-based Indirect Field-Oriented Control of IM Using PI-Fuzzy Logic Speed Controller

Rekha Tidke, Anandita Chowdhury

Department of Electrical Engineering, Sardar Vallabhbhai National Institute of Technology, Surat, India

Cite this article as: R. Tidke and A. Chowdhury, "Quasi ZSI-fed sliding mode control-based indirect field-oriented control of IM using PI-fuzzy logic speed controller," *Electrica*, 22(1), 70-83, Jan. 2022.

ABSTRACT

The demand for very efficient and top-performing power converters and drives is rising, which requires a new controlling strategy for the drive system. The induction motor (IM) and quasi-ZSI (q-ZSI) have elicited increasing interest in electric vehicle (EV) applications due to their unique features and benefits. However, it requires a perfect controlling scheme to reduce torque ripple and achieve a fast and dynamic IM response. The study in this paper has been carried out on a q-ZSI (impedance source inverter)-supplied IM drive. The PI controller, together with a fuzzy logic controller (FLC), is used as a speed regulator. The FLC with speed regulation reduces the torque ripple and SMC chattering of the IM. The sliding mode controller (SMC) replaces the two current PI controllers of indirect field-oriented control (IFOC). The proposed hybrid control strategy FLC–SMC–IFOC is implemented for the IM drive. The control system is implemented on the MATLAB/Simulink software and the results are compared with the conventional IFOC control. The proposed system results in improved dynamic response, minimized torque ripple, and fast convergence.
***Index Terms*—**Electric vehicle, indirect field-oriented control, induction motor, PI-fuzzy logic controller, sliding mode control.

I. INTRODUCTION

Presently, the global drive toward the reduction of greenhouse gas emissions for protection of the environment and to meet the advanced standards of fuel economy that have been proposed conserve the limited energy sources have made the development of electric vehicles (EVs) more crucial than ever. There is a lot of competition in the development of a propulsion drive motor for EVs. Currently, the most suitable motors for EV application are mainly the Permanent magnet synchronous motor (PMSM) and IM. Furthermore, the control technology with advanced power converters offers an attractive opportunity for the IM drive in the EV propulsion system. The industry faces more challenging technical conditions and restrictions, such as operating restrictions, which need to be addressed by the controller arrangement. The construction of Brushless DC (BLDC) and Permanent Magnet Synchronous Motor (PMSM) requires a permanent magnet (PM) on the rotor. This is expensive and needs to be imported. The recent Mahindra Reva e2o, Tesla model S, Tigor EV, Tesla Roadster, Mercedes Benz EQC, and the Toyota forklifts & buses use a three-phase IM in the power drivetrain. The IM drive is economical and best suitable for EV applications. The electromagnetic torque is kept close to its reference. The torque needs to be adjusted within a short transient response time of a few seconds to achieve good dynamic performance during torque transients. Such transients include torque changes of the load. If the machine's rotational speed is to be kept constant, the machine's torque should match the changing load torque to avoid speed fluctuations. On the other hand, the machine torque needs to be quickly adjusted to achieve fast changes in speed.

The q-ZSI offers a single-stage DC–DC–AC conversion without extra DC–DC conversion required like VSI. The q-ZSI has reduced the number of components, increased the efficiency, and reduced the volume with cost [1-6]. The q-ZSI network topology has eventually displayed its dominance over the ZSI on continuous current input, reduced stress on the source, and lower component rating. It has an extensive range of boosting voltage capability and is suitable for the EV. It also has increased applications in hybrid EVs (HEVs), fuel cells, photovoltaic panels, and PV arrays, discussed in [7-9]. In the traction motor for the EV/HEV propulsion system, the drive requirements are reliability, power density, low maintenance, low cost,

Corresponding Author:
Rekha Tidke

E-mail:
rstidke@gmail.com

Received: June 30, 2021

Revised: August 31, 2021

Accepted: September 9, 2021

Available Online Date: November 17, 2021

DOI: 10.5152/electrica.2021.21081

ruggedness, and mature technology. Permanent magnet rotors are tough to handle due to large forces that inherit play when anything ferromagnetic gets in contact with them. The PM motor magnet is very expensive. Therefore, the IM will likely hold a price benefit over PM machines. The IM seems to be the most adapted candidate for the electric propulsion for urban EV/HEV [10]. A control drive with the correct power converter is required for EVs to achieve a fast dynamic response. The SMC gives improved transient–dynamic response, robustness to parameter variation and external disturbances, and simplicity in implementation. The SMC decoupling controller-based IFOC IM drive for EV control gives a better dynamic performance, as discussed in [11,12]. Various advanced control techniques are presented in [13,14]. The electrical motors without magnet are the induction and synchronous wound field, which signify practical substitutes to PMSM or rare earth magnet motors in electric traction applications. The comparison between electric motors is addressed in [15,16].

Various literature shows the use of IM in EVs with different control methods. Direct torque control (DTC) and IFOC, in combination with SMC, fuzzy logic, genetic algorithm, and some observers, are proposed in [17-20]. The author in [21] presents a "self-governing motor" control assembly used in a propulsion system by the SMC speed regulator. Moreover, the SMC controls the driving wheel speed with high accuracy and improves the performance of the motors. In [22], a new control scheme of the four-wheel drive propulsion system control is introduced through innovative studies of SMC applied on EVs with four self-regulating wheels. The propulsion system contains four IMs and the EV uses an electronic differential for speed reference calculations of the four wheels. Different combinations of control methods are used along with the SMC approach for speed tracking, and low torque ripple is explained in [23-26]; however, it faces overshoot and high speed response time during load variations. The only use of a PI speed controller leads to a ripple in torque and flux with steady-state errors. In [27-29], advanced methods such as the conventional control techniques and advanced control techniques such as FLC and artificial neural network (ANN), PI-FLC, PI-SMC, and the ANN technique used for the control of IM for EV applications are presented. The IM has proved an appropriate solution for most industrial applications. Additionally, the control strategies offer the future of the sustainable automotive industry. The FLC is suitable for applications like electric vehicles, and industrial-purpose robotics. The FLC ensures the stable and improved operation in the IM drive with FLC. Some authors also report that FLC gives more vigorous and fast response and reduces the torque and flux ripples. Moreover, the FLC speed controller improves the overall transient response of the system [30-33]. Field-oriented control plays a vital role in IM control, which fulfills the power requirements of the EV power drive requirements. The FLC can minimize ripple contents in torque and flux. FLC can easily be tuned by fuzzy rules. Moreover, FLC with different rules can be introduced and FLC with 49 rules gives better performance. Different hybrid control strategies like MRAS-Fuzzy SMC and adaptive SMC are presented. The fuzzy-SMC scheme is efficient when compared to the SMC in eliminating the chattering phenomenon and improving response time. Adaptive SMC improves speed tracking effectively and improves dynamic response, as explained in [34-37]. In [38], a novel control approach for the speed control of IM fed by a bidirectional q-ZSI using the IFOC method is presented. A comparative study of the proper choice of the most appropriate electric propulsion system for a parallel HEV is described in [39]. The paper states that the advantages of the IM are maximum speed, high range of field weakening, low current at no load, no necessity for rare earth, robust design, absence of hazardous material, easy recycling, better safety with low effort, and low production costs. However, there are disadvantages like small torque density, higher weight and volume, and high current at constant torque. The mathematical modeling of the Induction motor and a basic matured controlled strategy with analysis are addressed in [40-42]. An EV requires a fast dynamic response and a wide speed range, with constant torque and constant power regions. Hence a new combined controller is implemented to achieve the requirement for an IM used in propulsion systems.

In the proposed control technique, the FLC regulates speed, reduces torque ripple, and eliminates the chattering phenomena of SMC over the entire speed range. An FLC combined with a PI speed regulator and an SMC-based IFOC produces a fast dynamic response with speed tracking and torque ripple reduction for various speeds and reduced load disturbances. The analytical calculation has also validated the finding. The results show a considerable minimization in torque ripple percentage. However, the speed convergence is fast and the overshoot is considerably reduced. Unlike conventional inverters, the ZSI can simultaneously offer boosting of input voltage applied and inversion action. The q-ZSI has voltage buck–boost abilities without an additional DC–DC converter, and provides the required voltage for the IM drive. The subsequent sections of the paper show the mathematical models for the IM and about q-ZSI, FLC, SMC control laws, SMC-based IFOC control strategy, and the MATLAB simulation results obtained with an IM drive.

II. DYNAMIC MODEL OF IM

The mathematical dynamic model of the three-phase IM represented in the d^e–q^e synchronously rotating reference are shown below in

$$V_{ds} = R_s i_{ds} + \frac{d\psi_{ds}}{dt} - \omega_e \psi_{qs}$$

$$V_{qs} = R_s i_{qs} + \frac{d\psi_{qs}}{dt} + \omega_e \psi_{ds} \quad (1)$$

$$\frac{d\psi_{dr}}{dt} = -\frac{R_r}{L_r}\psi_{dr} + \frac{R_r L_m}{L_r} i_{ds} + \omega_{sl}\psi_{qr}$$

$$\frac{d\psi_{qr}}{dt} = -\frac{R_r}{L_r}\psi_{qr} + \frac{R_r L_m}{L_r} i_{qs} - \omega_{sl}\psi_{dr} \quad (2)$$

$$T_e = \frac{3}{2}\frac{P}{2}\frac{L_m}{L_r}\left(\psi_{dr} i_{qs} - \psi_{qr} i_{ds}\right) \quad (3)$$

$$\frac{d\omega_m}{dt} = \frac{1}{J}[T_e - T_L - B\omega_m] \quad (4)$$

where V_{ds}, V_{qs}, i_{ds}, i_{qs}, ψ_{ds} and ψ_{qs} are stator direct axis and quadrature axis voltage, current, and flux respectively.ψ_{dr}, ψ_{qs} are rotor direct axis and quadrature axis flux. R_s, R_r, L_m, L_r, and P are stator resistance, rotor resistance, mutual inductance, rotor inductance, and pole pairs respectively of the IM motor parameters. Speed in rpm synchronous speed, rotor speed, and slip speed ω_e, ω_m, ω_{sl} are represented respectively. T_e, T_L, B, and J represent electromagnetic torque, load torque, viscous friction, and inertia respectively. With the help of indirect field-oriented control (IFOC) theory and using (2), slip calculation is done:

$$\psi_{qr} = 0 \tag{5}$$

$$\frac{d\psi_{qr}}{dt} = 0 \tag{6}$$

$$\omega_{sl} = \frac{i_{qs} R_r}{L_r i_{ds}} \tag{7}$$

$$\psi_{dr} = L_m i_{ds} \tag{8}$$

The traditional field-weakening technique based on $\frac{|\omega_b|}{|\omega_m|}$ is used:

$$i_{ds\_ref} = \frac{|\omega_b|}{|\omega_m|} i_{ds\_base} \tag{9}$$

From i_{ds_ref} direct axis rotor flux is calculated the using IFOC (8) as

$$\psi_{dr} = L_m i_{ds_{ref}}. \tag{10}$$

III. QUASI ZSI

The input current of the Z-source inverter (ZSI) is discontinuous, which will curtail the lifespan of the source battery pack and weaken the performance of the EV and HEV. The Z-source network components are rearranged, and a new topology is formed, that is, the quasi-ZSI (q-ZSI). The input current of the q-ZSI is continuous, while at the same time evoking all the merits of the ZSI, which makes it a good player for EV applications. The q-ZSI network contains two inductors *L*1 and *L*2, two capacitors *C*1 and *C*2, and a diode *D*, shown in Fig. 1. The q-ZSI is a power converter with a single-stage conversion that can achieve voltage buck–boost abilities and draw continuous input current from the battery source.

The q-ZSI modes of operation are categorized into three states. The first one is active, the second null, and the third is the shoot-through (ST) state. In the working of the active state, the q-ZSI works similar to a conventional voltage source inverter (VSI). All upper switches or lower switches of the inverter are conducted in the operation of the null state. Additionally, the ST state occurs when the upper and lower switches are turned on simultaneously on the same leg so that the inverter legs are one, two, or three short-circuited. There are 15 possible switching states in the q-ZSI. These states split into six active, two null, and seven ST states. The advantages of q-ZSI over VSI are given below:

(1) The main benefit of this network topology is that it can function as VSI or CSI, based on the use and requirements, and the output voltage of the q-ZSI can range from zero volts to any desired value.

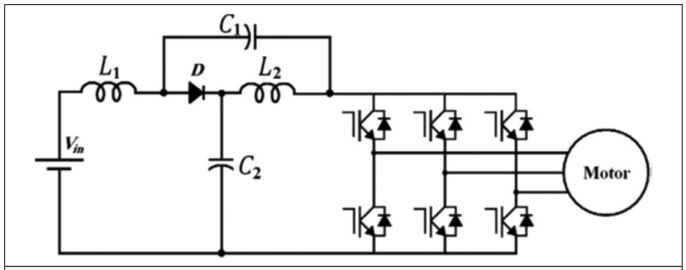

Fig. 1. Quasi ZSI topology [38].

(2) The ST state in ZSI offers a unique ability of buck–boost by changing the time of shoot-through for the inverter.
(3) It reduces the total component required and reduces passive component rating.
(4) It has continuous input current.
(5) It reduces the electric motor ratings to deliver essential power.
(6) It reduces in-rush and harmonic current when used in the adjustable speed drive, and also offers ride-through throughout voltage dips without any extra network and energy storage.
(7) It reduces volume due to the fewer number of components required and hence offers higher efficiency.

IV. SLIDING MODE – INDIRECT FIELD-ORIENTED CONTROL

For IFOC, the direct axis and quadrature axis current regulators that are required, which are responsible for flux and torque control respectively, are to be attuned, and these two currents are controlled by the sliding mode controller. Two sliding surfaces are required, s_1 and s_2, of which the first is for i_{ds} current control and the second is for i_{qs} current control, as given below:

$$s_1 = i_{ds\_ref} - i_{ds} \quad s_2 = i_{qs\_ref} - i_{qs} \tag{11}$$

where i_{ds_ref} and i_{qs_ref} are the values of the reference *d*-axis and reference *q*-axis stator currents, respectively, and i_{ds} and i_{qs} are the values of *d*-axis and *q*-axis stator currents respectively.

It is required to design a control law, as the output of the current regulator is nothing but direct axis stator voltage and quadrature axis stator voltage [22]:

$$V_{ds} = V_{ds}^{equ} + V_{ds}^{n}$$

$$V_{qs} = V_{qs}^{equ} + V_{qs}^{n} \tag{12}$$

The voltage discontinuous control V_{ds}^{n} and V_{qs}^{n} is defined as

$$V_{ds}^{n} = k_1\, sat\left(\frac{s_1}{\varphi_1}\right)$$

$$V_{qs}^{n} = k_2\, sat\left(\frac{s_2}{\varphi_2}\right) \tag{13}$$

$$sat\left(\frac{s_1}{\varphi_1}\right) = \begin{cases} \frac{s_1}{\varphi_1}; & if \left|\frac{s_1}{\varphi_1}\right| < 1 \\ sign\left(\frac{s_1}{\varphi_1}\right); & if \left|\frac{s_1}{\varphi_1}\right| > 1 \end{cases}$$

$$sat\left(\frac{s_2}{\varphi_2}\right)=\begin{cases}\dfrac{s_2}{\varphi_2}; & if\left|\dfrac{s_2}{\varphi_2}\right|<1\\ sign\left(\dfrac{s_2}{\varphi_2}\right); & if\left|\dfrac{s_2}{\varphi_2}\right|>1\end{cases} \tag{14}$$

where k_1, k_2 are positive constants and constant factors φ_1, φ_2 are the boundary layer values. To reduce the chattering problem which occurs due to the signum (signs) function, the saturation (sat) function is used in voltage discontinuous control. The equivalent voltage control law V_{qs}^{equ} is defined with help from mathematical modeling of IM and IFOC theory:

$$\frac{di_{ds}}{dt}=\frac{1}{L_s\sigma}\left[V_{ds}-\left[R_s+\frac{L_m{}^2}{t_rL_r}\right]i_{ds}+\frac{L_m}{L_r}\frac{1}{t_r}\psi_{dr}+L_s\sigma\omega_e i_{qs}\right] \tag{15}$$

$$\frac{di_{qs}}{dt}=\frac{1}{L_s\sigma}\left[V_{qs}-\left[R_s+\frac{L_m{}^2}{t_rL_r}\right]i_{qs}-\frac{L_m}{L_r}\omega_m\psi_{dr}-L_s\sigma\omega_e i_{ds}\right] \tag{16}$$

where $\sigma=\left[1-\frac{L_m{}^2}{L_sL_r}\right]$ and $t_r=\frac{L_r}{R_r}$.

The derivative of sliding surface s_1 and s_2 is given below

$$\dot{s_1}=\dot{i}_{ds\_ref}-\dot{i}_{ds}$$

$$\dot{s_2}=\dot{i}_{qs\_ref}-\dot{i}_{qs}. \tag{17}$$

The equivalent control law part obtained by taking $s_1 = 0$ and $s_2 = 0$ is

$$V_{ds}^{equ}=L_s\sigma\left[\dot{i}_{ds_{ref}}+\frac{1}{L_s\sigma}\left[R_s+\frac{L_m{}^2}{t_rL_r}\right]i_{ds}+\frac{1}{L_s\sigma}\frac{L_m}{L_r}\frac{1}{t_r}\psi_{dr_{ref}}+\omega_e i_{qs}\right]$$

$$V_{qs}^{equ}=L_s\sigma\left[\dot{i}_{ds_{ref}}+\frac{1}{L_s\sigma}\left[R_s+\frac{L_m{}^2}{t_rL_r}\right]i_{qs}+\frac{1}{L_s\sigma}\frac{L_m}{L_r}\omega_m\psi_{dr\_ref}+\omega_e i_{ds}\right]. \tag{18}$$

V. FUZZY LOGIC CONTROLLER

The FLC is one of the controllers of AI techniques. The design of FLC starts by assigning the expected input and output variables. Fuzzification is the control method of changing a mathematical variable to convert to a fuzzy variable (linguistic number). After fuzzification, fuzzy rules apply with the help of fuzzy reasoning, then defuzzification is done with the support of the centroid formula, which gives a crisp value as output.

For continuous membership function (MF), for example, the defuzzified value represented as a^* using center of gravity (centroid) is defined as follows:

$$a^*=\frac{\int a\,MF(a)da}{\int MF(a)da}. \tag{19}$$

The triangular MFs are used to define fuzzy sets. In the fuzzy MF, $ei_{qs\_ref(k)}$ and $e^*i_{qs\_ref(k)}$ are the two inputs. Every input has seven MFs. Hence, the probable 49 FLC rules [29] are shown in the Table I, and the FLC rules with reasoning are shown in Fig. 2. The negative large, medium, small by *NL*, *NM*, and *NS* respectively, zero as ZE and positive large, medium, small by *PL*, *PM*, *PS* respectively are shown in Table I.

Similarly, FLC is implemented for direct axis current control along with the basic field-weakening method, so that proper control on current change is achieved. The FLC provides more controlled stator current for further control action in the drive as shown in Fig. 3. These two controlled current values are applied for achieving voltage equivalent control law values:

$$V_{ds}^{equ}=L_s\sigma\left[\dot{i}_{ds\_FL}+\frac{1}{L_s\sigma}\left[R_s+\frac{L_m{}^2}{t_rL_r}\right]i_{ds}+\frac{1}{L_s\sigma}\frac{L_m}{L_r}\frac{1}{t_r}\psi_{dr_{ref}}+\omega_e i_{qs}\right] \tag{20}$$

$$V_{qs}^{equ}=L_s\sigma\left[\dot{i}_{qs\_FL}+\frac{1}{L_s\sigma}\left[R_s+\frac{L_m{}^2}{t_rL_r}\right]i_{qs}+\frac{1}{L_s\sigma}\frac{L_m}{L_r}\omega_m\psi_{dr\_ref}+\omega_e i_{ds}\right] \tag{21}$$

VI. PROPOSED SYSTEM

In conventional IFOC of IMs, the required proportional-integral (PI) controller for regulation of speed and two more PI controllers for stator current along the direct axis provides flux control, and stator current along quadrature axis provides torque control, controller output provides a controlled voltage which is applied to q-ZSI via the space vector pulse width modulation (SVPWM) technique. The slip speed calculation is done with the benefits of an IFOC theory. In the proposed control scheme, the speed PI controller combined with the FLC is implemented to achieve fast tracking, reduce torque ripple, and reduce chattering action in the sliding mode controller. Similarly, the traditional field weakening has been implemented to weaken

TABLE I. FUZZY MEMBERSHIP FUNCTIONS [26]

$ei_{qs\_ref(k)}$ / $e^*i_{qs\_ref(k)}$	***NL***	***NM***	***NS***	***ZE***	***PS***	***PM***	***PL***
NL	*NL*	*NL*	*NL*	*NL*	*NM*	*NS*	*ZE*
NM	*NL*	*NL*	*NL*	*NM*	*NS*	*ZE*	*PS*
NS	*NL*	*NL*	*NM*	*NS*	*ZE*	*PS*	*PM*
ZE	*NL*	*NM*	*NS*	*ZE*	*PS*	*PM*	*PL*
PS	*NM*	*NS*	*ZE*	*PS*	*PM*	*PL*	*PL*
PM	*NS*	*ZE*	*PS*	*PM*	*PL*	*PL*	*PL*
PL	*ZE*	*PS*	*PM*	*PL*	*PL*	*PL*	*PL*

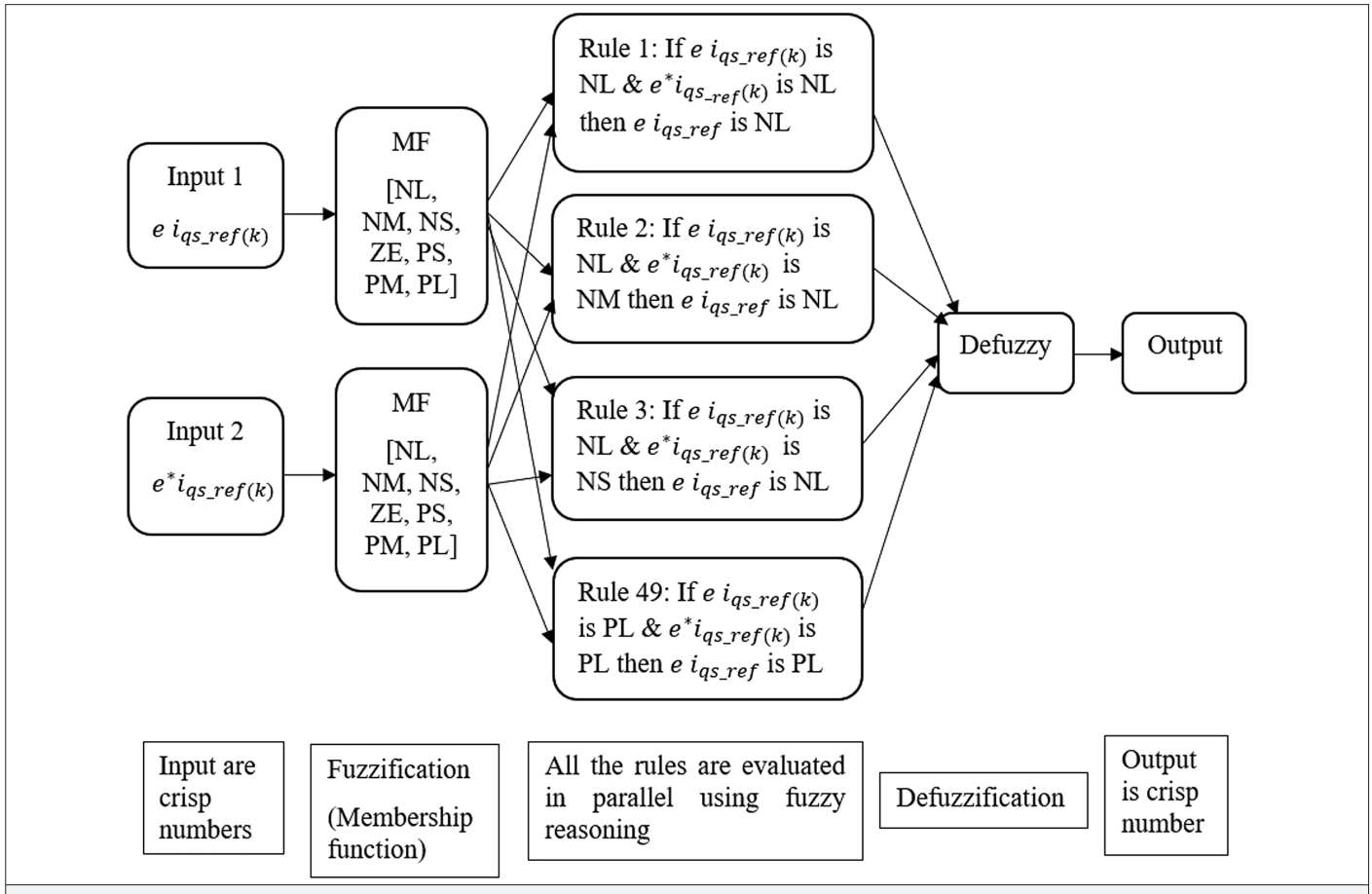

Fig. 2. Fuzzy logic rules.

the flux for higher speeds, and also to get direct axis stator current reference and more controlled value with the support of the FLC. The fuzzy logic (FL) with SMC-IFOC control gives better performance and a low ripple in torque, flux, stator current, and fast speed tracking. In the SMC controller, the two-control laws are designed that give controlled stator direct axis and quadrature axis voltages. The proposed system diagram is shown in Fig. 4. The use of fuzzy logic-controlled output currents and the chattering phenomena are not seen in the sliding mode controller, and torque fluctuation of the IM is reduced. The voltage control equivalent values have been obtained accurately, and, hence accurate stator voltages have been obtained. The SMC-IFOC-controlled stator voltages have been applied to space vector pulse width modulation after inverse park transformation to obtain pulses for q-ZSI. Here, a three-phase squirrel cage induction motor with 4 poles, 4 kW, and a rated speed of 1430 rpm is used and the applied pulses are of 5 kHz switching frequency.

VII. COMPARATIVE PERFORMANCE ANALYSIS

A. Comparative Performance Analysis in Speed Operation

In this performance analysis, three case studies are analyzed using a constant reference speed with constant load toque and step reference speed with constant load torque for both control methods with the MATLAB Simulink, and the resulting simulation waveform.

1) Case I Constant Torque and Constant Speed

In this case, both techniques run for rated speed of 1430 rpm and with 5 Nm load torque T_L, in simulation speed waveform,

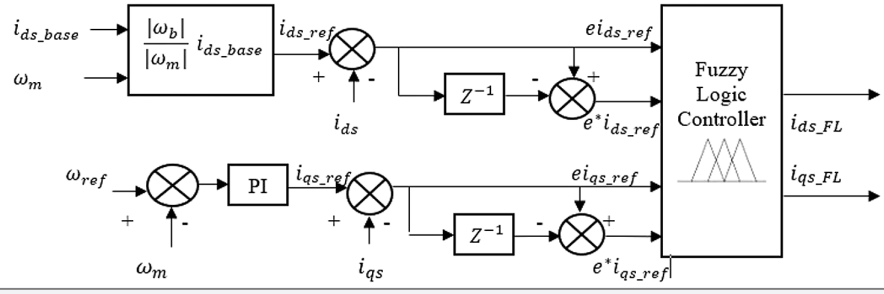

Fig. 3. Proposed schematic of fuzzy logic controller.

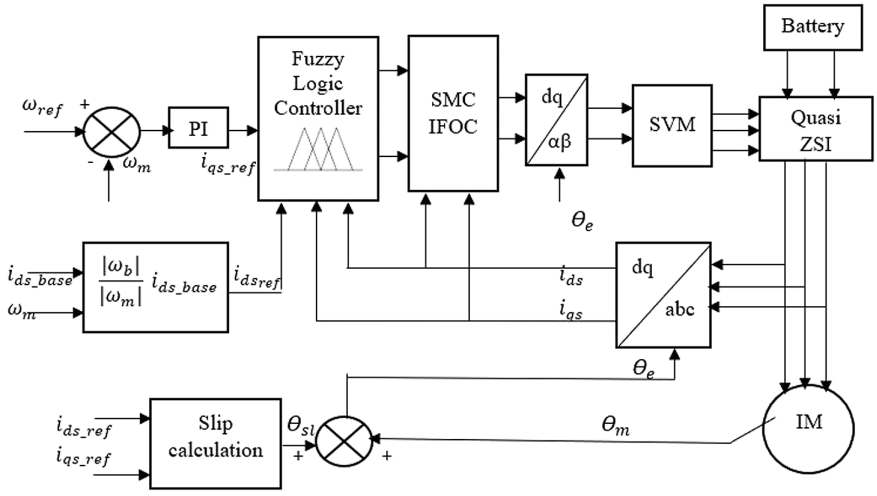

Fig. 4. Proposed control system.

as shown in Fig. 5. The rise time taken by the proposed control method is less that is 0.22 seconds, with peak overshoot of 22 rpm and undershoot of 7 rpm, and speed convergence is observed at 0.3 seconds, whereas in conventional IFOC, the rise time taken is 0.25 seconds with peak overshoot of 34 rpm and undershoot of 51 rpm, and speed convergence observed at 0.6 seconds, as shown in Fig. 5. It is observed that the proposed control technique achieved fast dynamic transient response by the considering the above three factors. In torque waveform also, the proposed control method converges faster when compared to the IFOC control method, as shown in zoom view when torque at 0.25 seconds and at 0.45 seconds reaches 5 Nm respectively. Torque ripple in the IFOC method is 17.91%, while in the proposed system it is 9.72% respective to applied load torque of 5 Nm.

It is observed from the current and flux waveform that the proposed system gives smooth waveform with less ripple as compared to the IFOC method shown in Fig. 6 and 7. By analytical calculation, the percentage torque ripple at various speeds and torques is shown in Table II, it is observed that torque ripple is significantly reduced in the proposed control method as compared to the IFOC control method. Also, speed and torque fluctuation are present in IFOC control method at high speed and high torque, which are eliminated by the proposed method.

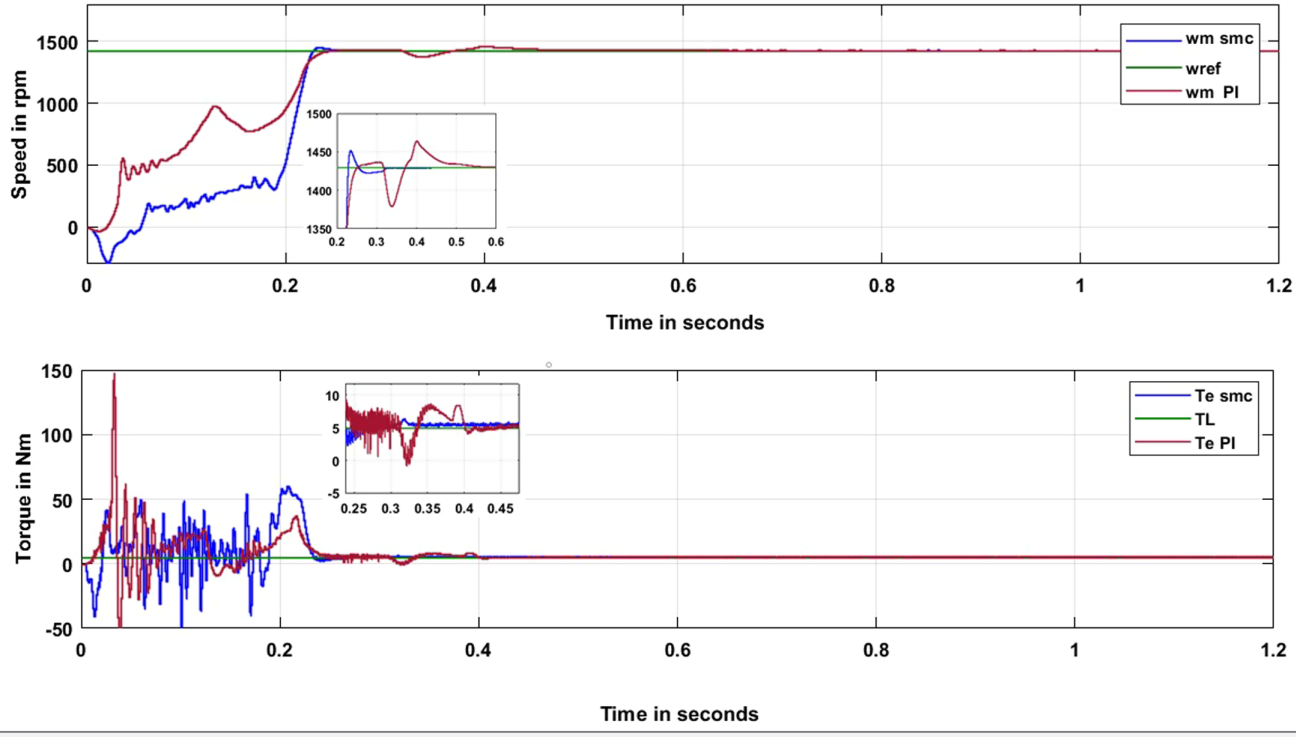

Fig. 5. Speed and torque response at speed operation.

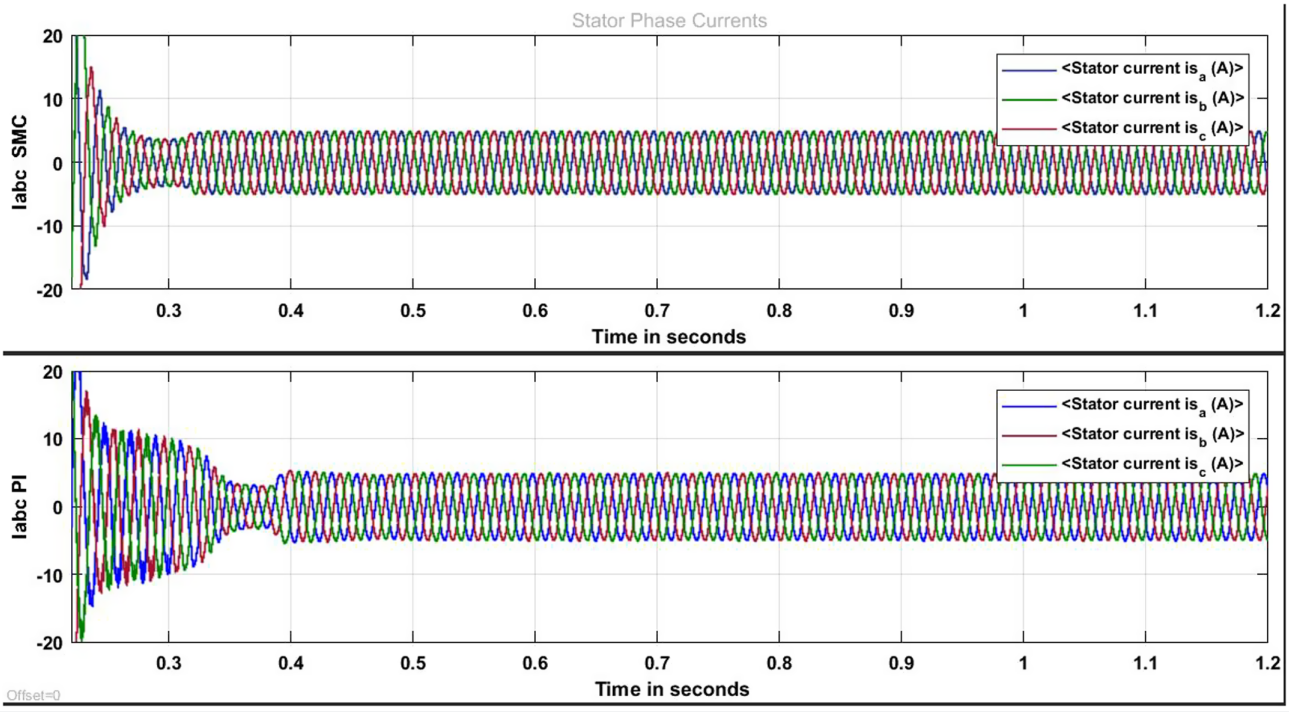

Fig. 6. Stator current response at speed operation.

The results also revealed that the percentage reduction in torque ripples have been significantly lower with the proposed method for rated and higher speeds, as summarized in Table II.

2) Case II Constant Torque and Step Speed

In this case, both techniques for the IM run for constant 5 Nm load torque T_L and the step reference speed input signal is provided starting from a low speed of 1000 rpm, increasing to the rated speed of 1430 rpm, and then to a higher speed of 1800 rpm, and further decreased from the higher to the rated speed and to low speed again. In simulation speed waveform, zoom view is shown at each step to check speed tracking and fast speed convergence which is considerably less in the proposed control method. In torque waveform, at each step response little more spike observed can been

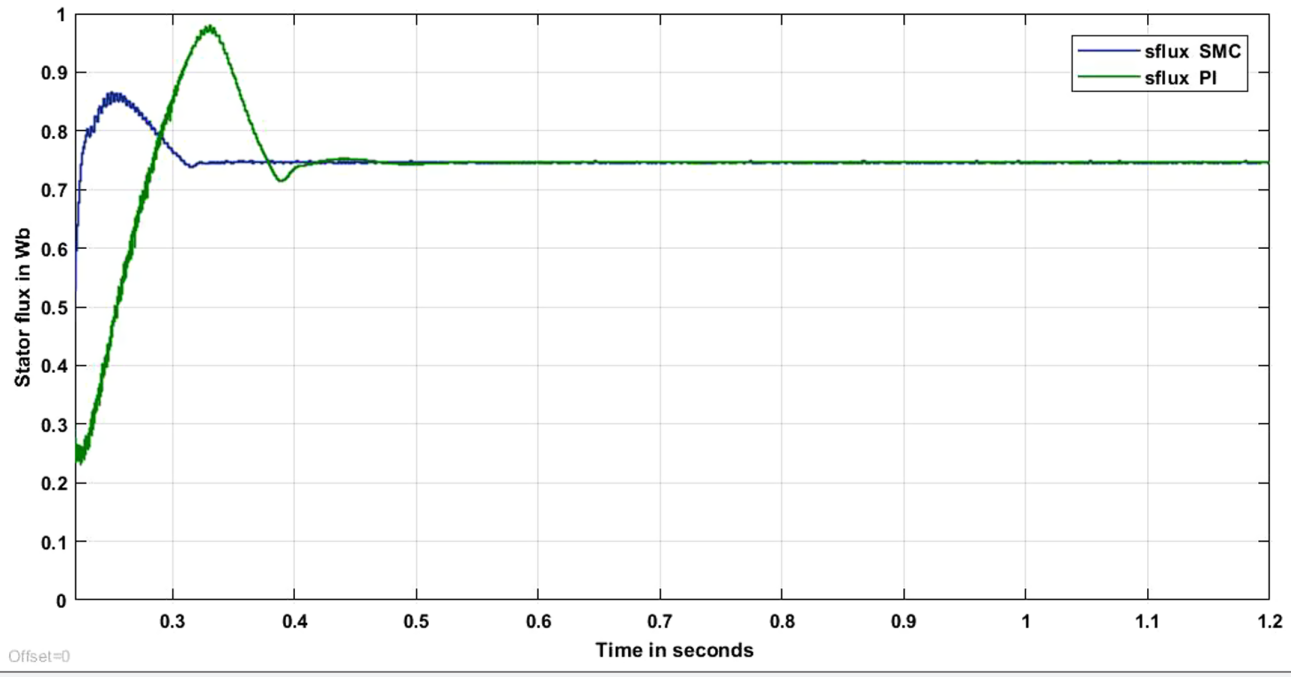

Fig. 7. Stator flux at speed operation.

TABLE II. TORQUE RIPPLE PERCENTAGE IN CASE I

		Percentage Torque Ripple	
Speed in rpm	**Load Torque in Nm**	**Proposed Control Method**	**IFOC Control Method**
1000	15	2.3096	2.6634
	20	1.6979	1.8933
	25	1.4105	2.3359
1430	15	3.2578	12.3086
	20	3.145	9.5385
	25	3.0554	7.5928
1800	15	7.5497	17.2238
	20	6.7401	12.5638
	25	5.9416	10.4107

seen in zoom view in case of the proposed control technique but the convergence is fast as compared to the PI-IFOC method. The proposed system shows the current smooth waveform, in Fig. 8 and 9 showing speed and torque dynamic response with time at different speed ranges. Also shown is the corresponding stator current response at speed operation.

It has been observed from the performed analysis that the convergence of speed as well as torque is faster with the proposed method. Moreover, the rise time and the overshoot in this case are also comparatively better. The results also reveal that the performance of the proposed method is much better for the cases of constant speed and step speed from rated to high speed. However, for the case of low to rated speed, the performance is noted to be consistent with that of the IFOC control method, as summarized in Table III.

It has been observed that the percentage of torque ripples is reduced in further operating conditions, as shown in the analysis presented in Table IV. However, the reduction in this case is comparatively lower than that observed in case of constant speed operation. From the performed analysis, in terms of the smoothness of motor operation under variable speed and torque, the measured oscillations are more in the IFOC method. However, the magnitude of oscillations is noted to increase with the increase in the applied torque.

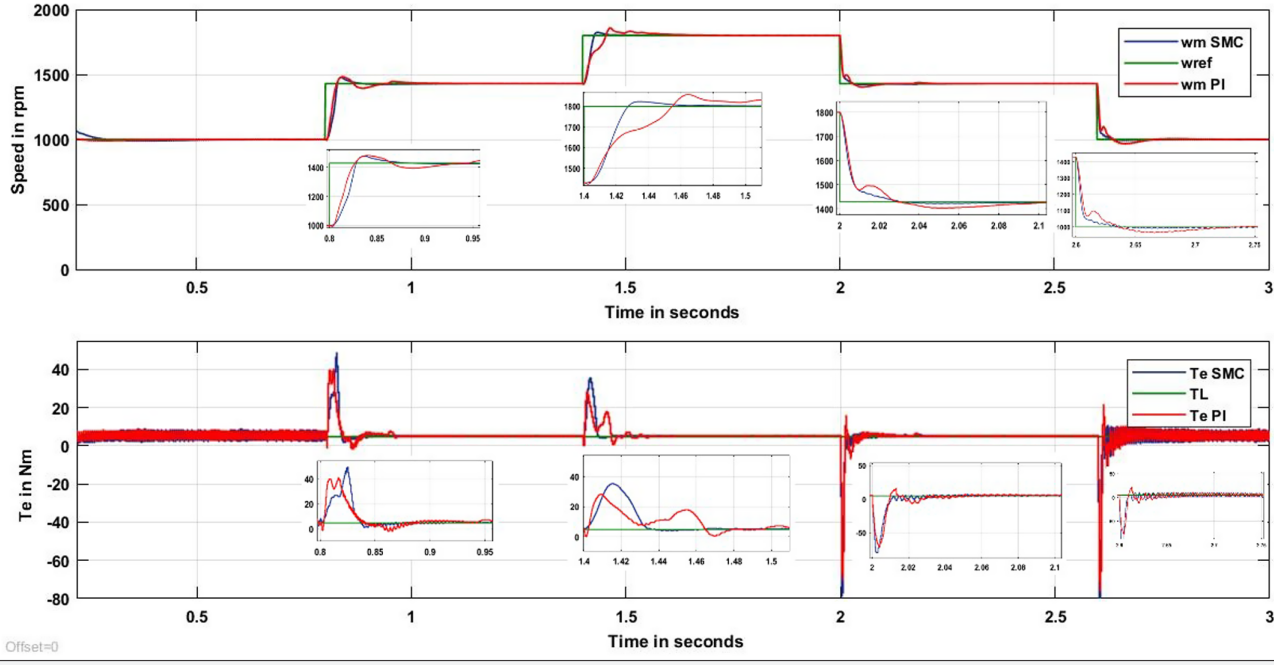

Fig. 8. Speed and torque response at step speed operation.

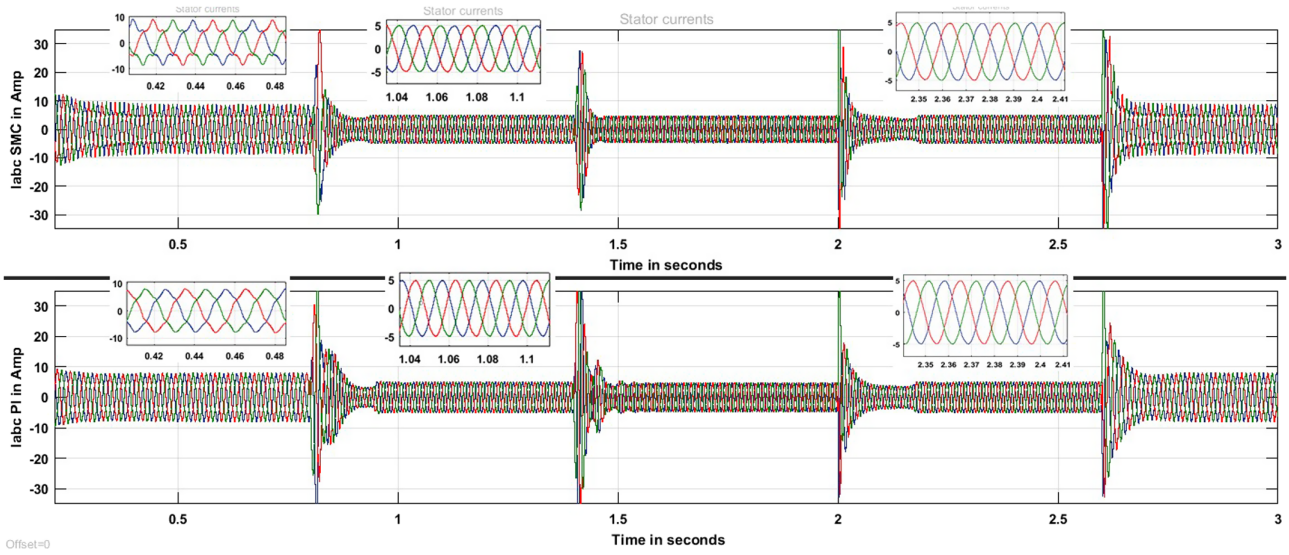

Fig. 9. Stator current response at speed operation.

B. Comparative Performance Analysis Under Torque Variation

In this performance analysis, a rated speed of 1430 rpm is used with an initial load torque of 5 Nm. The step torque or variable load torque gradually increases to 10 Nm and then to 15 Nm, and again decreases gradually from 15 Nm to 10 Nm and finally to 5 Nm under constant speed for both control schemes. The applied load torque T_L and the electromagnetic torque T_e of both SMC-IFOC and PI-IFOC systems are shown Fig. 10 and 11. It is observed from the speed waveform in SMC-IFOC system, that speed shows fast convergence with less time and less drop in speed during load changes as compared to the PI-IFOC system.

1) Case III Rated Speed and Step Torque

The comparative performance analysis during load variations is summarized in Table V. The results reveal that drops in the speed are insignificant with an increase in load, and are found consistent for both of these methods. However, the speed convergence is faster in the proposed method.

TABLE III. SUMMARY OF COMPARATIVE ANALYSIS IN SPEED OPERATION

Case	Dynamic Parameter	Proposed Control Method	IFOC Control Method
Constant speed 1430 rpm and constant torque 5 Nm	Overshoot (rpm)	22	34
	Undershoot (rpm)	7	51
	Rise time (s)	0.22	0.25
	Speed convergence time (s)	0.3	0.6
	Torque convergence time (s)	0.25	0.45
Low speed to rated speed with load torque 5 Nm	Overshoot (rpm)	48	48
	Undershoot (rpm)	7	35
	Rise time (s)	0.828	0.826
	Speed convergence time (s)	1.15	1.16
	Torque convergence time (s)	0.85	1
Rated speed to high speed with load torque 5 Nm	Overshoot (rpm)	25	55
	Undershoot (rpm)	No	No
	Rise time (s)	1.425	1.455
	Speed convergence time (s)	1.5	1.7
	Torque convergence time (s)	1.44	1.55

TABLE IV. TORQUE RIPPLE PERCENTAGE UNDER DIFFERENT OPERATING CONDITIONS

		Percentage Torque Ripple	
Step Speed in rpm	**Load Torque in Nm**	**Proposed Control Method**	**IFOC Control Method**
1000–1430	15	2.7310	3.2289
	20	2.0622	2.6115
1430–1800	15	3.8737	4.3059
	20	3.5822	3.6766
1800–1430	15	2.5630	2.7238
	20	1.4153	1.4360
1430–1000	15	1.9638	2.2514
	20	1.3127	1.5941

TABLE V. SUMMARY OF COMPARATIVE ANALYSIS AT RATED SPEED

Case	**Dynamic Parameter**	**Proposed Control Method**	**IFOC Control Method**
Load torque from 5 Nm to 10 Nm with rated speed	Drop in speed (rpm) when load changes	20	19
	Speed convergence time (s)	1.14	1.23
	Torque convergence time (s)	0.95	1
Load torque from 10 Nm to 15 Nm with rated speed	Drop in speed (rpm) when load changes	26	23
	Speed convergence time (s)	1.8	1.85
	Torque convergence time (s)	1.77	1.8
Load torque from 15 Nm to 10 Nm with rated speed	Drop in speed (rpm) when load changes	26	25
	Speed convergence time (s)	2.3	2.5
	Torque convergence time (s)	2.15	2.2
Load torque from 10 Nm to 5 Nm with rated speed	Drop in speed (rpm) when load changes	19	22
	Speed convergence time (s)	2.93	2.95
	Torque convergence time (s)	2.72	2.8

The performance analysis during no load to full load under different speed conditions is presented in Table VI. The analysis is considered for three different constant speed operations with the zero to rated load. It has been observed that in a case of low speed with zero to rated load, the drop in speed is considerable along with the better convergences of speed and torque.

For the cases of rated and higher speed, the drop in speed has been noted to be significant. However, for the higher loading conditions of the motor, the speed and torque are found to be oscillatory in nature. The findings of the performed analysis with both the control methods are summarized in Table VII.

VIII. CONCLUSION

In this paper, the hybrid control method is proposed for the induction motor drive. It has been shown from MATLAB/ Simulink results that the proposed control scheme gives robust and better dynamic transient responses suitable for EV /HEV application. The proposed control technique attained fast speed convergence to different signals of reference speed and exhibited good robustness to load variations. The SMC doesn't show chattering problems due to the use of FLC. The desired voltage range obtained due to the q-ZSI-fed system also optimizes cost. The performance analysis of the IFOC of the IM drive and SMC-based IFOC with PI-fuzzy logic of the IM drive

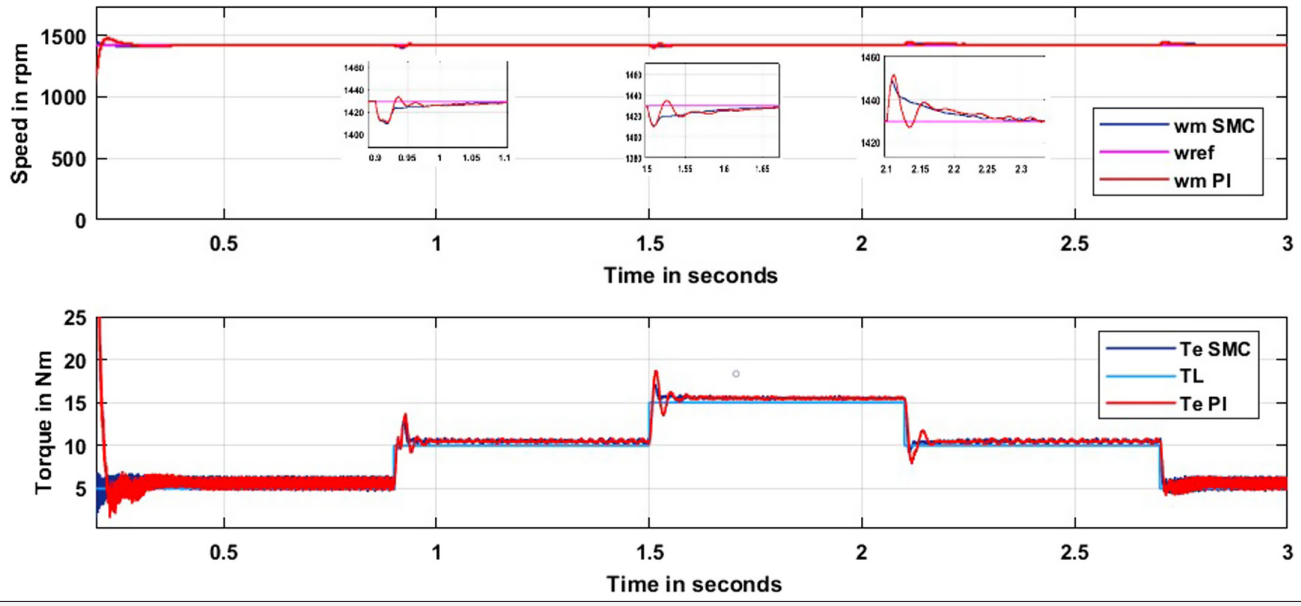

Fig. 10. Speed and torque response at load variation.

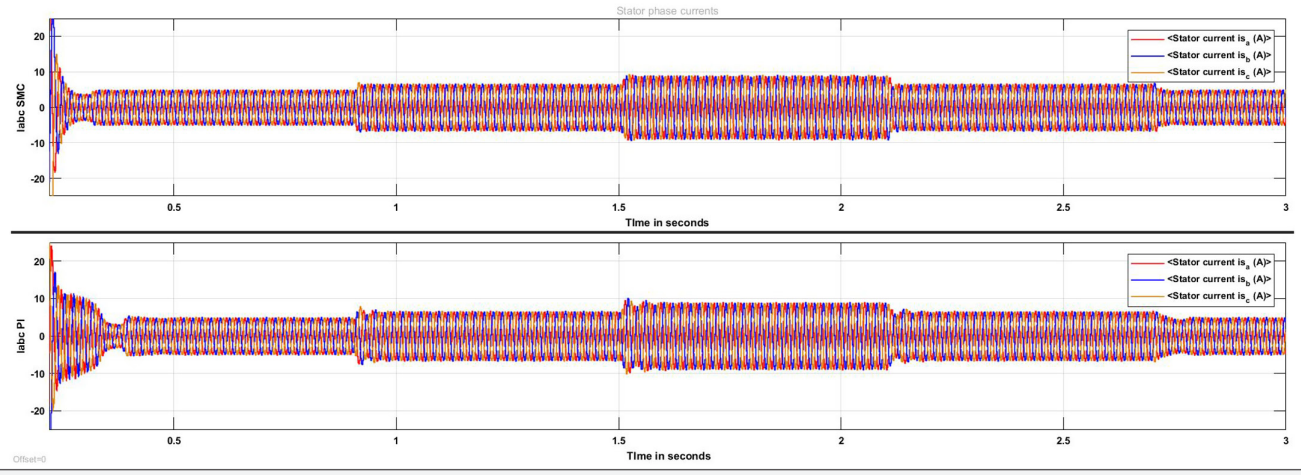

Fig. 11. Stator current response at load variation.

TABLE VI. PERFORMANCE ANALYSIS DURING NO LOAD TO FULL LOAD UNDER DIFFERENT SPEED CONDITION

Case	Dynamic Parameter	Proposed Control Method	IFOC Control Method
1000 rpm with step torque 0 Nm to 25 Nm	Drop in speed (rpm) when load changes	60	80
	Speed convergence time (s)	0.8	0.9
	Torque convergence time (s)	0.6	0.7
Rated speed with step torque 0 Nm to 25 Nm	Drop in speed (rpm) when load changes	70	110
	Speed convergence time (s)	0.8	Not converged
	Torque convergence time (s)	0.6	Not converged
1800 rpm with step torque 0 Nm to 25 Nm	Drop in speed (rpm) when load changes	34	80
	Speed convergence time (s)	0.8	Not converged
	Torque convergence time (s)	0.7	Not converged

TABLE VII. PERFORMANCE ANALYSIS SUMMARY

Sr. No.	Dynamic Parameter	Proposed Control Method	Conventional IFOC Method
1	Speed convergence time	Fast	Slow
2	Rise time	Less	Moderate
3	Overshoot	Small	High
4	Speed response time after load applied	Fast	Slow
5	Drop in speed when load applied	Less	Moderate
6	Torque response time at speed change	Fast	Slow

is evaluated based on various dynamic parameters like rising time, overshoot, speed convergence, and speed drop when load variation and torque ripple occur. The proposed system achieved a considerable reduction in percentage torque ripple. Moreover, it achieved fast speed convergence over a wide range of speed and load variations.

Peer-review: Externally peer-reviewed.

Author Contributions: Concept – R.T., A.C.; Design – R.T., A.C.; Supervision – R.T., A.C.; Data Collection and/or Processing – R.T., A.C.; Analysis and/or Interpretation – R.T., A.C.; Literature Search – R.T., A.C.; Writing Manuscript – R.T., A.C.; Critical Review – R.T., A.C.

Conflict of Interest: The authors have no conflicts of interest to declare.

Financial Disclosure: The authors declared that this study has received no financial support.

REFERENCES

1. F. Z. Peng, "Z-source inverter," *IEEE Trans. Ind. Appl.*, vol. 39, no. 2, pp. 504–510, 2003. [CrossRef]
2. F. Z. Peng *et al.*, "Z-source inverter for motor drives," *IEEE Trans. Power Electron.*, vol. 20, no. 4, pp. 857–863, 2005. [CrossRef]
3. F. Z. Peng, M. Shen, and K. Holland, "Application of Z-source inverter for traction drive of fuel cell—Battery hybrid electric vehicles," *IEEE Trans. Power Electron.*, vol. 22, no. 3, pp. 1054–1061, 2007. [CrossRef]
4. W. P. Q. Tong, B. M. S. M. Ramadan, and T. Logenthiran, "A comparative analysis between Z-source and quasi-Z-source inverters for boost operation," in *Asian Conf. Energy Power Transp. Electrification (ACEPT)*, 2018, pp. 1–6. [CrossRef]
5. T. Maity and H. Prasad, "Real-time performance evaluation of quasi Z-source inverter for induction motor drives," in *26th Int. Symp. Ind. Electron. (ISIE)*, 2017, pp. 844–849. [CrossRef]
6. Y. P. Siwakoti, F. Z. Peng, F. Blaabjerg, P. C. Loh, and G. E. Town, "Impedance-source networks for electric Power conversion Part I: A topological review," in *IEEE Trans. Power Electron.*, vol. 30, no. 2, pp. 699–716, Feb. 2015. [CrossRef].
7. K. Beer and B. Piepenbreier, "Properties and advantages of the quasi-Z-source inverter for DC-AC conversion for electric vehicle applications," in *Emobility – Electr. Power Train*, 2010, pp. 1–6. [CrossRef]
8. S. Rahman, K. Rahman, M. A. Ali, M. Meraj, and A. Iqbal, "Quasi Z source inverter fed V/f controlled five phase induction motor drive powered," in *Int. Conf. Electr. Electron. Comput. Eng. (UPCON)*, 2019, pp. 1–6. [CrossRef]
9. S. T. Telrandhe, S. S. Pande, and S. V. Umredkar, "Performance analysis of solar fed electronically commutated motor driven water pump using ZSI and q-ZSI," in *3rd Int. Conf. Comput. Methodol. Commun. (ICCMC)*, 2019, pp. 157–161. [CrossRef]
10. M. Zeraoulia, M. E. H. Benbouzid, and D. Diallo, "Electric motor drive selection issues for HEV propulsion systems: A comparative study," *IEEE Trans. Veh. Technol.*, vol. 55, no. 6, pp. 1756–1764, 2006. [CrossRef]
11. M. Muhammad, Z. Rasin, and A. Jidin, "Bidirectional quasi-Z-source inverter with hybrid energy storage for IM drive system," in *9th Symp. Comput. Appl. Ind. Electron. (ISCAIE)*, 2019, pp. 75–80. [CrossRef]
12. M. Farasat, A. M. Trzynadlowski, and M. S. Fadali, "Efficiency improved sensorless control scheme for electric vehicle induction motors," *IET Electr. Syst. Transp.*, vol. 4, no. 4, pp. 122–131, 2014.
13. T. Wang, P. Zheng, Q. Zhang, and S. Cheng, "Design characteristics of the induction motor used for hybrid electric vehicle," *IEEE Trans. Magn.*, vol. 41, no. 1, pp. 505–508, 2005. [CrossRef]
14. N. El Ouanjli *et al.*, "Modern improvement techniques of direct torque control for induction motor drives: A review," *Prot. Control Mod. Power Syst.*, vol. 4, no. 1, p. 11, 2019. [CrossRef]
15. C. P. Gor, V. A. Shah, and M. P. Gor, "Electric vehicle drive selection related issues," in *Int. Conf. Signal Process. Commun. Power Embed. Syst. (SCOPES)*, 2016, pp. 74–79. [CrossRef]
16. M. Popescu, J. Goss, D. A. Staton, D. Hawkins, Y. C. Chong, and A. Boglietti, "Electrical vehicles—Practical solutions for power traction motor systems," *IEEE Trans. Ind. Appl.*, vol. 54, no. 3, pp. 2751–2762, 2018. [CrossRef]
17. X. Zhang, "Sensorless induction motor drive using indirect vector controller and sliding-mode observer for electric vehicles," *IEEE Trans. Veh. Technol.*, vol. 62, no. 7, pp. 3010–3018, 2013. [CrossRef]
18. A. Hazzab, I. K. Bousserhane, and M. Kamli, "Design of a fuzzy sliding mode controller by genetic algorithms for induction machine speed control," *Int. J. Emerg. Electr. Power Syst.*, vol. 1, no. 2, 2004.
19. A. Saghafinia, H. W. Ping, M. N. Uddin, and K. S. Gaeid, "Adaptive fuzzy sliding-mode control into chattering-free IM drive," *IEEE Trans. Ind. Appl.*, vol. 51, no. 1, pp. 692–701, 2015. [CrossRef]
20. A. Ghezouani, B. Gasbaoui, and J. Ghouili, "Modeling and sliding mode DTC of an EV with four in-wheel induction motors drive," in *Int. Conf. Electr. Sci. Tech. Maghreb (CISTEM)*, 2018, pp. 1–9. [CrossRef]
21. N. Abdelfatah, H. Abdeldjebar, I. Bousserhane, S. Hadjeri, and P. Sicard, "Two wheel speed robust sliding mode control for electric vehicle drive," *Serb. J. Electr. Eng.*, vol. 5, no. 2, pp. 199–216, 2008. [CrossRef]
22. A. Ghezoua, B. Gasbaoui, and J. Ghouili, "Sliding mode control for four wheels electric vehicle drive," in *9th Int. Conf. Interdiscipl. Eng.*, 2015. [CrossRef]
23. R. Solea, M. Gaiceanu, and V. Nicolau, "Sliding mode controller for induction motor," in *4th Int. Symp. Electr. Electron. Eng. (ISEEE)*, 2013, pp. 1–5. [CrossRef]
24. A. Ltifi, M. Ghariani, and R. Neji, "Performance comparison of PI, SMC and PI-sliding mode controller for EV," in *15th Int. Conf. Sci. Tech. Auto. Control Comput. Eng. (STA)*, 2014, pp. 291–297. [CrossRef]
25. I. Sami, S. Ullah, A. Basit, N. Ullah, and J. -S. Ro, "Integral super twisting sliding mode based sensorless predictive torque control of induction motor," *IEEE Access*, vol. 8, pp. 186740–186755, 2020. [CrossRef]

26. N. Goel, R. N. Patel, and S. Chacko, "Torque ripple reduction of the DTC IM drive using artificial intelligence," in *Int. Conf. Electr. Power Ener. Syst. (ICEPES)*, 2016, pp. 5–9. [CrossRef]
27. H. Mediouni, S. El Hani, M. Ouadghiri, I. Aboudrar, and I. Ouachtouk, "Artificial intelligence techniques for induction motor drives," in *IEEE Int. Electr. Mach. Drives Conf. (IEMDC)*, 2017, pp. 1–6. [CrossRef]
28. M. Aktas, K. Awaili, M. Ehsani, and A. Arisoy, "Direct torque control versus indirect field-oriented control of induction motors for electric vehicle applications," *Eng. Sci. Technol. An Int. J.*, vol. 23, no. 5, 1134–1143, 2020.
29. T. Ramesh and A. K. Panda, "Direct flux and torque control of three phase induction motor drive using PI and fuzzy logic controllers for speed regulator and low torque ripple," in *Stud. Conf. Eng. Syst.*, 2012, pp. 1–6. [CrossRef]
30. V. R. Metha and S. S. Karvekar, "Speed control of induction motor using a fuzzy logic controller and direct torque controller," in *4th Int. Conf. Converg. Tech. (I2CT)*, 2018, pp. 1–5. [CrossRef]
31. N. V. Uma Maheswari and L. J. Sahaya Shanthi, "Performance improvement of sensorless induction motor drive with fuzzy logic controller," in *2nd Int. Conf. Intel. Comput. Control Syst. (ICICCS)*, 2018, pp. 591–596. [CrossRef]
32. V. S. Virkar and S. S. Karvekar, "Luenberger observer-based sensorless speed control of induction motor with Fuzzy tuned PID controller," in *Int. Conf. Commun. Electr. Syst. (ICCES)*, 2019, pp. 503–508. [CrossRef]
33. A. Bitoleanu, C. V. Suru, and M. Linca, "Fuzzy speed control in drive systems with voltage inverters and induction motors," in *6th Int. Symp. Electr. Electron. Eng. (ISEEE)*, 2019, pp. 1–6. [CrossRef]
34. G. Joshi and A. J. Pinto Pius, "Type-1 Mamdani fuzzy logic controller for electric vehicle drive," in *Int. Conf. Smart Syst. Invent. Tech. (ICSSIT)*, 2019, pp. 224–229. [CrossRef]
35. S. Ali, S. A. R. Kashif, H. Q. Ali, and K. Toqueer, "Direct torque control of inverter fed three phase induction motor by implementing fuzzy logic controller," in *6th Int. Conf. Eng. Tech. Appl. Sci. (ICETAS)*, 2019, pp. 1–8. [CrossRef]
36. D. Fereka, M. Zerikat, and A. Belaidi, "MRAS sensorless speed control of an induction motor drive based on fuzzy sliding mode control," in *7th Int. Conf. Syst. Control (ICSC)*, 2018, pp. 230–236. [CrossRef]
37. C. S. T. Dong, C. D. Tran, S. D. Ho, P. Brandstetter, and M. Kuchar, "Robust sliding mode observer application in vector control of induction motor," in *ELEKTRO*, 2018, pp. 1–5. [CrossRef]
38. O. Ellabban and H. Abu-Rub, "Indirect field oriented control of an induction motor fed by a bidirectional quasi Z-source inverter," *IECON 2012 - 38th Ann. Conf. IEEE Ind. Electron. Soc.*, 2012, pp. 5297–5302. [CrossRef]
39. D. Zechmair, and K. Steidl, "Why the induction motor could be the better choice for your electric vehicle program," *World Electr. Veh. J.*, vol. 5, no. 2, pp. 546–549, 2012. [CrossRef]
40. B. K. Bose, *Modern Power Electronics and AC Drives*. Upper Saddle River, NJ, USA: Prentice Hall PTR, 2002, vol. 8, ch. 2. ISBN 0-13-016743-6.
41. M. H. Rashid, *Power Electronics Handbook*. Oxford, U.K.: Butterworth-Heinemann, 2001, ch. 33. ISBN 13: 978-0-12-088479-7. ISBN 10: 0-12-088479-8.
42. P. C. Krause, *Analysis of Electrical Machinery and Drive Systems*. Hoboken, NJ, USA: Wiley, 2013, ch. 4. ISBN: 978-1-118-02429-4.

Rekha Tidke has received her B.E. and M.E. degrees from the K. K. Wagh College of Engineering, Nashik, under the university of Pune, India. She is presently working as Assistant Professor in the Department of Electrical Engineering of Gokhale Education society R. H. Sapat College of Engineering, Nashik. She is pursuing a Ph.D. degree in the Electrical Engineering Department at S.V. National Institute of Technology, Surat in India, from Dec 2018. Her research interests include electrical machines, drives, and power electronics, and their applications in the electric vehicle.

Anandita Chowdhury received her B.E. and M.E. degrees from the University of Calcutta, and her Ph.D. degree from the Indian Institute of Technology, Kharagpur. Presently, she is working as Professor in the Department of Electrical Engineering of S. V. National Institute of Technology, Surat, India. She has more than twenty-five years of teaching experience. Her areas of research interest include electrical machines, drives, and power system stability

APPENDIX A

Squirrel cage Induction motor parameters

Mutual inductance $L_m = 0.172$ H; Stator inductance $L_s = 0.178$ H;

Rotor inductance $L_r = 0.178$ H; Stator resistance $R_s = 1.405\ \Omega$;

Rotor resistance $R_r = 1.395\ \Omega$; Pole pairs $P = 2$

Output power $P_n = 4$ kW; Line voltage $V_L = 400$ V;

Supply frequency $f_s = 50$ Hz; Maximum load torque $T_L = 25$ Nm

Rotor rated speed $N_r = 1430$ rpm; Inertia $J = 0.0131$ kg m^2